

Muon sites in PbF_2 and YF_3 : decohering environments and the role of anion Frenkel defects

J. M. Wilkinson,^{1,*} F. L. Pratt,² T. Lancaster,³ P. J. Baker,² and S. J. Blundell^{1,†}

¹*Clarendon Laboratory, University of Oxford Department of Physics,
Parks Road, Oxford, OX1 3PJ, United Kingdom*

²*ISIS Facility, STFC Rutherford Appleton Laboratory, Didcot OX11 0QX, United Kingdom*

³*Centre for Materials Physics, Durham University, Durham DH1 3LE, United Kingdom*

(Dated: September 1, 2021)

Muons implanted into ionic fluorides often lead to a so-called $\text{F}-\mu-\text{F}$ state, in which the time evolution of the muon spin contains information about the geometry and nature of the muon site. Nuclei more distant from the muon than the two nearest-neighbor fluorine ions result in decoherence of the $\text{F}-\mu-\text{F}$ system and this can yield additional quantitative information about the state of the muon. We demonstrate how this can be applied to the determination of muon sites within the ionic fluorides $\alpha\text{-PbF}_2$ and YF_3 which contain fluoride ions in different crystallographic environments. Our results can be used to distinguish between different crystal phases and reveal the presence of anion Frenkel defects in $\alpha\text{-PbF}_2$.

Muon spin rotation (μSR) is a technique which involves implanting spin-polarized positive muons (lifetime $\tau_\mu = 2.2 \mu\text{s}$) in samples to probe the local magnetic environment [1, 2]. This technique has been applied very successfully to measure vortices in superconductors [3], explore the ground states in magnetic materials [4, 5], probe the physics of hydrogen-like defect states in semiconductors [6–8] and in many other situations. In order to quantitatively analyze the data obtained from μSR experiments, one needs to know the final stopping site of the implanted muon within the crystal, *and* the extent to which the muon perturbs the local crystallographic and electronic structure. Density functional theory (DFT) calculations have recently been used to address this question [9–11]. The muon is placed at a randomly chosen site in the unit cell and the structure relaxed, with all atoms and the muon allowed to move until convergence is reached and the final energy evaluated; repeating this for many initial muon positions and identifying the minimum energy configuration yields an estimate of the muon site and allows the local distortions of the structure to be identified. This method is often referred to as “DFT+ μ ”.

Ionic fluorides are a useful class of materials for the study of muon stopping sites and the muon-induced perturbation on the local crystallographic environment [9, 12]. Fluorine, being the most electronegative element [13], is a very attractive atom for the incoming μ^+ and, in ionic fluorides, the muon commonly stops between two fluorine anions, adopting a $\text{F}-\mu-\text{F}$ state, somewhat analogous to a bifluoride ion (HF_2^-). Following implantation, the muon spin becomes entangled with the spins on nearest-neighbour fluorine nuclei, and the muon’s polarization then evolves with time as governed by the magnetic dipolar Hamiltonian, producing a characteristic beating oscillatory signal in the measured positron asymmetry [12, 14] that allows the muon site to be identified. The muon’s polarization also decoheres into the environment (the spin system consisting of all the other nuclei

in the compound), becoming lost in an irreversible process, which causes a relaxation in the beating oscillatory signal. It has been shown very recently that this can be quantitatively modelled to produce excellent agreement with experimental data in the simple cubic fluorides CaF_2 and NaF [15].

In this letter, we extend the method used for CaF_2 and NaF [15], and apply it to two ionic fluorides: YF_3 [16] and $\alpha\text{-PbF}_2$. These were chosen as they have structural phases with a more complicated structure than the simple cubic phases considered previously, and thereby show that this method can be utilized in conjunction with DFT+ μ to provide an insight into structural phase transitions and defect states, allowing us to gain a fuller understanding of the nature of the perturbation of the muon on the surrounding nuclei.

When a muon is implanted in a sample, it interacts with the surrounding nuclear spins by means of the dipole-dipole Hamiltonian \mathcal{H} , given by

$$\mathcal{H} = \sum_{i>j} \frac{\mu_0 \gamma_i \gamma_j}{4\pi \hbar |\mathbf{r}_{ij}|^3} \left[\mathbf{s}_i \cdot \mathbf{s}_j - 3(\mathbf{s}_i \cdot \hat{\mathbf{r}}_{ij})(\mathbf{s}_j \cdot \hat{\mathbf{r}}_{ij}) \right], \quad (1)$$

where \mathbf{r}_{ij} is the vector linking spins i and j , and all other symbols having their usual meanings. For the case of a muon interacting with spin- $\frac{1}{2}$ fluorine (^{19}F) nuclei ($\gamma_{\text{F}} = 2\pi \times 40.061 \text{ MHz T}^{-1}$), the muon’s polarization then evolves in an observable pattern of beats (the frequencies of which provide information of the surrounding nuclei, due to the \mathbf{r}_{ij} dependence of the Hamiltonian), with a relaxation which is due to the system decohering with the environment of further nearest-neighbours, which have a weaker, but non-negligible coupling to the muon. Including all the nuclei in the sample directly in Eq. (1) is not possible since the dimension of \mathcal{H} grows exponentially with the number of spins included. Therefore, following [15] we cut off our Hilbert space to include enough nearest-neighbours to describe the main features of the μSR asymmetry, and then rescale the coupling to

the k ions most distant to the muon using a parameter ζ_k which is chosen so that the second moment of our reduced system matches that of the infinite system. The variance of the field distribution at the muon caused by M spins is $(\sigma_M/\gamma_\mu)^2 = \frac{2}{3} \left(\frac{\mu_0}{4\pi}\right)^2 \hbar^2 \sum_{j=1}^M \gamma_j^2 I_j(I_j + 1)/r_j^6$, where r_j is the distance from the muon to the j^{th} nucleus with spin I_j and gyromagnetic ratio γ_j , $\gamma_\mu (= 2\pi \times 135.5 \text{ MHz T}^{-1})$ is the muon gyromagnetic ratio, and the sum converges as $M \rightarrow \infty$. We then calculate ζ_k from

$$\sigma_\infty^2 = \sigma_{\text{nn}}^2 + \frac{2}{3} \left(\frac{\mu_0}{4\pi}\right)^2 \hbar^2 \gamma_\mu^2 \sum_{j \in k} \frac{\gamma_j^2 I_j(I_j + 1)}{(\zeta_k r_j)^6}, \quad (2)$$

and then evaluate our exact calculation of the muon polarization to the restricted set of muon, nearest-neighbours and the set of k ions (with interaction strength rescaled by ζ_k).

In many fluorides, an additional relaxation component is also present in the μSR asymmetry. The origin of this component has up until now been unidentified, but we believe that in PbF_2 this is due to diamagnetic Mu^- states located in anion vacancies, the origin of which are due to anion Frenkel defects (AFDs). The likelihood of AFDs forming is quantified by the defect formation energy, g_{F} , which usually is of the order of a few eV, meaning that a large abundance of these defects often occur in equilibrium at temperatures of the order of hundreds of kelvin, and some can be frozen into the material and still be present at low temperatures. We therefore utilized DFT to estimate the anion Frenkel defect formation energy, with an approach similar to that undertaken before in pyrochlores [17]: We created a supercell composed of $2 \times 2 \times 2$ conventional unit cells, and one of the anions was displaced to a new site of high symmetry, and the cell relaxed. The location of the defects which had the lowest energy are shown in Fig. 1. We found that if the anion is placed in an interstitial site sufficiently far away from the the vacancy, the atoms would not relax to their original positions. The final relaxed energies of the supercells containing the defect were compared to those without defects to obtain an estimate for g_{F} , and these energies are tabulated in Table I, alongside the experimental values where available, which agree well with our calculations. From this, one can conclude that both structural phases of PbF_2 are much more likely to contain Frenkel defects than YF_3 and CaF_2 , a result which is supported by the absence of evidence of such defect states in those compounds in our μSR experiments.

We obtained samples of both YF_3 and PbF_2 commercially, and used an X-Ray diffractometer to confirm that they did not contain any significant impurities (see Supplemental Information) and that the PbF_2 sample adopted the α -phase. These samples were then wrapped in silver foil measured with the MuSR spectrometer at the ISIS facility [21]. The muon decay asymmetry was calculated from the number of counts in the forward and

Compound	g_{F} (eV) (calculated)	g_{F} (eV) (experimental)
YF_3	3.70	-
CaF_2	2.17	2.2–3.1 [18, 19]
$\alpha\text{-PbF}_2$	1.55	1.12 [20]
$\beta\text{-PbF}_2$	1.05	0.9–1.1 [18, 20]

TABLE I. Anion Frenkel defect energies g_{F} calculated by DFT (also showing the experimental values where available, using the method described in the text.

backward detectors.

High statistics data were collected for both YF_3 and PbF_2 (274 and 358 million decay events, respectively).

The stopping sites of the muon were calculated using DFT+ μ for YF_3 , and both the α and β phases of PbF_2 (see Supplemental Information for details). The sites which had the lowest overall energy are depicted in Fig.1 [22] The stopping sites of the Mu^- ions in the vacancies caused by the AFDs were also calculated and are shown in the figure; they were found to be very close to the positions of the anion vacancies, as expected.

The PbF_2 data were fitted with the function

$$A(t) = A_{\text{r}}[(1 - c_{\text{AFD}})P^\mu(r_{\text{nn1}}, r_{\text{nn2}}, \zeta_4; t) + c_{\text{AFD}}P^{\text{Mu}^-}(t)] + A_{\text{bg}}e^{-(\lambda t)^2} \quad (3)$$

assuming the α phase and also, to test the robustness of the procedure, assuming the β phase. The first term $P^\mu(\dots)$ describes the muon polarization calculated from the dipolar Hamiltonian (1), using the muon site calculated with DFT+ μ , where r_{nn1} and r_{nn2} represent the distance from the muon to the two nearest neighbour fluorines. The second term $P^{\text{Mu}^-}(t)$ is the polarization of the negatively charged Muonium ion in an AFD site, and the final term $e^{-(\lambda t)^2}$ represents a slow relaxation of the muon polarization due to the weak nuclear moments in the Ag sample holder. As Pb has a very weak moment (the only isotope with spin, ^{207}Pb , has $\mu = 0.584\mu_{\text{N}}$ with 23% abundance), only the nearest ten fluorine nuclei were included in the calculation of the muon polarisation (see the Supplemental Information for the positions of the included nuclei) and so the Hamiltonian was described by a matrix of size 2048×2048 .

The results of the fits to both the α and β phases are shown in Fig. 2(a), along with simulations for which c_{AFD} was fixed to zero (i.e. ignoring AFDs). From this, one can see that the best fit is obtained including the presence of AFDs and with PbF_2 adopting the α phase. The superiority of the α -phase fit is especially apparent for the data at longer times ($> 8 \mu\text{s}$), where the polarization function strongly deviates from the data for the β phase. Further evidence supporting the validity of the model applying to the α phase of the compound is obtained by considering the second moment rescaling factor ζ . The fit for the α

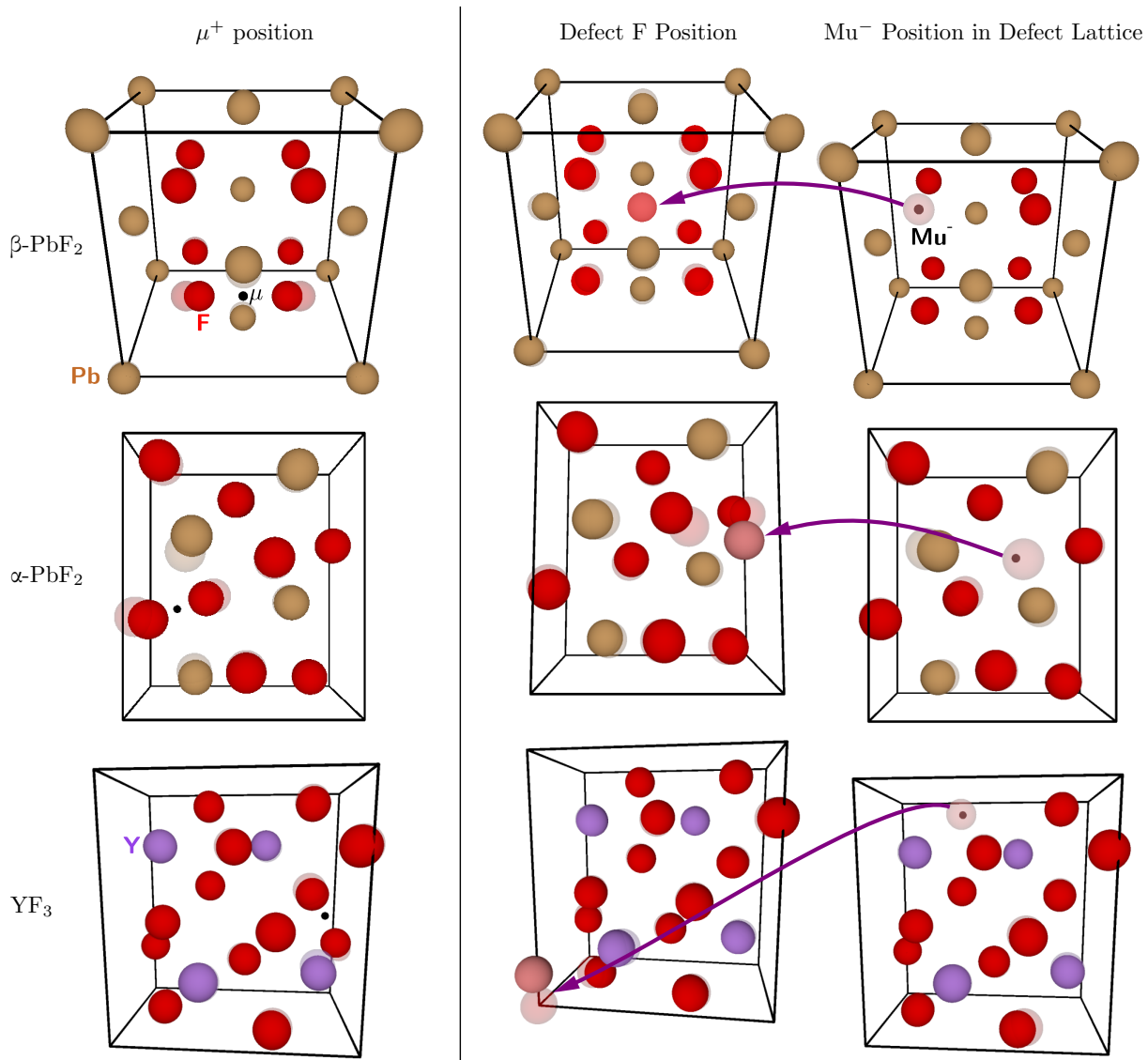


FIG. 1. Muon sites in PbF_2 and YF_3 , calculated with DFT. The left-hand side shows the muon site calculated with the DFT+ μ method, as described in the text. In all cases, the muon (black sphere) sits in between two fluoride ions (red spheres), and the transparent (solid) spheres show the locations of the surrounding ions before (after) the perturbation of the implanted muon. The centre column shows the position of the defect fluorine in the perfect lattice, and the final (initial) relaxed positions of the surrounding ions are displayed as solid (transparent) spheres. Finally, the right-hand column shows the site of the Mu^- (black sphere) in the vacancy created by such a defect, and the effect of this on the surrounding ions.

phase obtained a value of $\zeta_4 = 0.834(5)$, very close to the calculated value of 0.8433. However, for the β phase, the fitted value of $\zeta_{\text{nnn}} = 0.804(4)$, strongly deviating from the calculated value of 0.8956. For the α phase, the final obtained values of r_{nn1} and r_{nn2} were 1.1419(4) Å and 1.2601(7) Å, close to the corresponding values of 1.10 and 1.21 Å obtained with DFT+ μ . These results therefore demonstrate that the details of the oscillatory signal are able to correctly distinguish between the two related crystallographic phases of PbF_2 , but note that the sen-

sitivity of μSR data to these local differences is only revealed clearly in the late-time data (obtained well after $\approx 5\tau_\mu$ where, because of the muon decay, the data rate is more than two orders of magnitude lower than that obtained immediately after implantation). This result highlights the necessity for obtaining high-statistics μSR data so that these small late-time features in the data can be carefully resolved.

The best fit to the zero-field data was obtained assuming that 9.2(2)% of the diamagnetic fraction of the signal

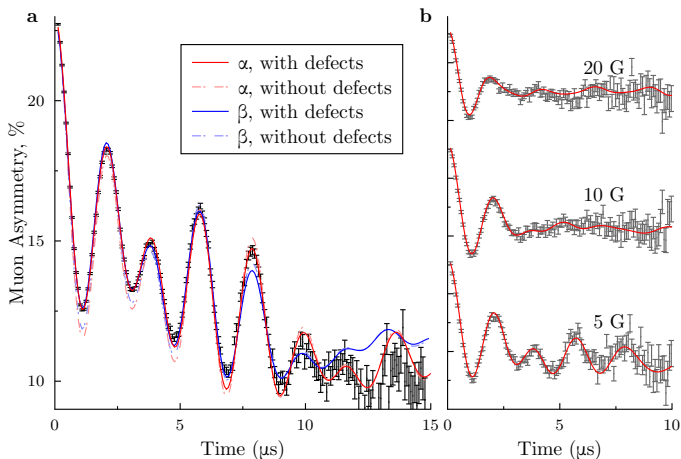


FIG. 2. α - PbF_2 Results. **a** shows the zero-field μSR data obtained for our sample of PbF_2 , and the solid (dashed) lines corresponding to fits of the data with (without) taking into account the Mu^- entering into a defect state. **b** shows the data obtained with a longitudinal field applied, plotted with the muon polarization as described in the text.

in α - PbF_2 was due to AFD states. In order to test for the presence of these states, we applied a series of small longitudinal fields to the sample. Applying such fields adds an additional Zeeman term to the Hamiltonian, which, for AFD Mu^- states, tends to be much larger than the dipole interactions, and hence $P^{\text{Mu}^-}(t) \approx 1$. These results, along with plots of the polarization function for α - PbF_2 , using parameters obtained from the aforementioned fit and with no further adjustment of parameters, apart from including the longitudinal field, are shown in Figure 2(b). One can see that our model continues to describe the data very well, and the field indeed removes much of the effect of the defect states on the polarization.

As our data for YF_3 did not show any slow relaxing background, and the DFT results show that AFDs are less likely to form than in PbF_2 , we did not need to include AFDs in our fits of the data. Therefore we fit our YF_3 data to a simpler functional form, given by

$$A(t) = A_r P^\mu(r_{\text{nn}1}, r_{\text{nn}2}, r_{\text{nnn}1}, r_{\text{nnn}2}, \zeta_6; t) + A_{\text{bg}}, \quad (4)$$

where $r_{\text{nnn}1}$ and $r_{\text{nnn}2}$ are the distances between the muon and the two next-nearest neighbour fluorine nuclei, and all other symbols have the same meaning as before. As with PbF_2 , the ten nearest fluorine nuclei were included in the calculation (Y has only one natural isotope, ^{89}Y , with a negligible moment of $0.137\mu\text{N}$), leading again to matrices of size 2048×2048 (see the Supplemental Information for the details of the included nuclei). The site which was predicted by DFT to have the lowest energy (using both the LDA and PBE functionals) was used to calculate the muon polarization, the fit of which is depicted as the green line in Figure 3. The values obtained from the fit, and their DFT counterparts, are tabulated in

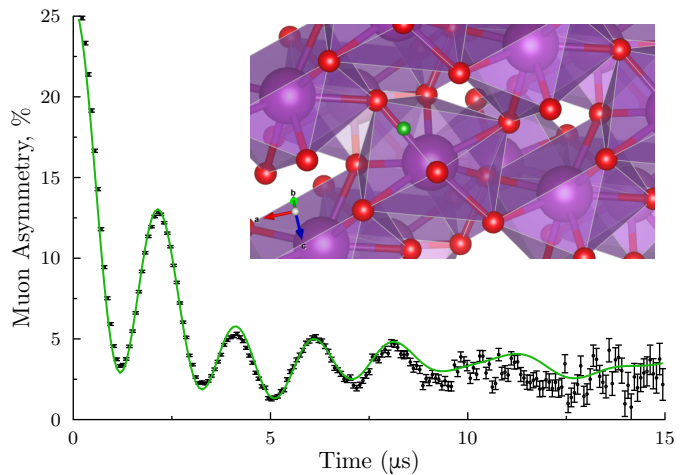


FIG. 3. YF_3 Results: The results of our μSR experiment, with the fitted muon polarization using the muon site obtained by DFT. This site is displayed on the YF_3 crystal structure in the inset, with the atom positions unperturbed for simplicity.

Parameter	Experimental	DFT+ μ	Difference
$r_{\text{nn}1}$ (\AA)	1.173(1)	1.10	+0.073
$r_{\text{nn}2}$ (\AA)	1.278(2)	1.22	+0.058
$r_{\text{nnn}1}$ (\AA)	2.24(3)	2.15	+0.09
$r_{\text{nnn}2}$ (\AA)	2.40(1)	2.49	-0.09
ζ_6	0.849(5)	0.907	-0.058

TABLE II. Muon-induced structural distortions in YF_3 , comparing the values obtained with the fit to experimental data with the values obtained using DFT+ μ .

Table II, where it can be seen that the nearest- and next-nearest- neighbour perturbations of the fluorines due to the muon are in excellent agreement. Note that the discrepancy between the DFT values and the fitted values increases with the muon-fluorine distance, and that DFT slightly underestimates the bond lengths for nuclei close to the muon, and slightly overestimates these for those nuclei further away. While the PBE functionals tend to slightly underestimate bond lengths, the effect further from the muon may be due to the size of the supercell.

In conclusion, we have shown how the analysis of μSR data on complex fluorides allows one to obtain a wealth of useful information about the muon stopping site and the environment of the muon, information which was previously not obtainable when phenomenological relaxation functions were used to analyze the data. We have also shown how the longer-time data are particularly useful for understanding the nature of the muon site. Additionally, we have shown that it is possible to measure anion Frenkel defects using μSR in a model system, an important result which can be extended to the analysis

of magnetic systems, where the effects of defects on the electronic structure could be important.

We acknowledge support from EPSRC (Grant No. EP/N023803/1) and the use of the University of Oxford Advanced Research Computing (ARC) facility in carrying out this work (<http://dx.doi.org/10.5281/zenodo.22558>). We are grateful to D. Prabhakaran for performing the x-ray measurement and to Marina Filip for useful discussions. Part of this work was carried out at the STFC-ISIS muon facility.

* john.wilkinson@physics.ox.ac.uk

† stephen.blundell@physics.ox.ac.uk

- [1] S. J. Blundell, Spin-polarized muons in condensed matter physics, *Contemporary Physics* **40**, 175 (1999).
- [2] S. J. Blundell, R. De Renzi, T. Lancaster, and F. L. Pratt, eds., *Introduction to Muon Spectroscopy* (Oxford University Press, Oxford, 2021).
- [3] J. E. Sonier, J. H. Brewer, and R. F. Kiefl, μ sr studies of the vortex state in type-II superconductors, *Rev. Mod. Phys.* **72**, 769 (2000).
- [4] P. D. de Réotier and A. Yaouanc, Muon spin rotation and relaxation in magnetic materials, *J. Phys.: Condens. Matter* **9**, 9113 (1997).
- [5] F. L. Pratt, P. J. Baker, S. J. Blundell, T. Lancaster, S. Ohira-Kawamura, C. Baines, Y. Shimizu, K. Kanoda, I. Watanabe, and G. Saito, Magnetic and non-magnetic phases of a quantum spin liquid, *Nature* **471**, 612 (2011).
- [6] B. D. Patterson, Muonium states in semiconductors, *Rev. Mod. Phys.* **60**, 69 (1988).
- [7] S. F. J. Cox, Muonium as a model for interstitial hydrogen in the semiconducting and semimetallic elements, *Rep. Prog. Phys.* **72**, 116501 (2009).
- [8] K. Shimomura and T. U. Ito, Electronic structure of hydrogen donors in semiconductors and insulators probed by muon spin rotation, *J. Phys. Soc. Jpn.* **85**, 091013 (2016).
- [9] J. S. Möller, D. Ceresoli, T. Lancaster, N. Marzari, and S. J. Blundell, Quantum states of muons in fluorides, *Phys. Rev. B* **87**, 121108 (2013).
- [10] F. Bernardini, P. Bonfà, S. Massidda, and R. De Renzi, Ab initio strategy for muon site assignment in wide band gap fluorides, *Phys. Rev. B* **87**, 115148 (2013).
- [11] P. Bonfà and R. De Renzi, Toward the computational prediction of muon sites and interaction parameters, *J. Phys. Soc. Jpn.* **85**, 091014 (2016).
- [12] T. Lancaster, S. J. Blundell, P. J. Baker, M. L. Brooks, W. Hayes, F. L. Pratt, J. L. Manson, M. M. Conner, and J. A. Schlueter, Muon-fluorine entangled states in molecular magnets, *Phys. Rev. Lett.* **99**, 267601 (2007).
- [13] A. L. Allred, Electronegativity values from thermochemical data, *J. Inorg. Nucl. Chem.* **17**, 215 (1961).
- [14] J. H. Brewer, S. R. Kreitzman, D. R. Noakes, E. J. Ansaldo, D. R. Harshman, and R. Keitel, Observation of muon-fluorine “hydrogen bonding” in ionic crystals, *Phys. Rev. B* **33**, 7813 (1986).
- [15] J. M. Wilkinson and S. J. Blundell, Information and decoherence in a muon-fluorine coupled system, *Physical Review Letters* **125**, 087201 (2020).
- [16] Although YF_3 has been measured and analyzed before [10], the crystal structure used for the analysis was incorrect, and it was therefore not possible to fit the data without including a phenomenological relaxation function.
- [17] W. R. Panero, L. Stixrude, and R. C. Ewing, First-principles calculation of defect-formation energies in the $\text{Y}_2(\text{Ti},\text{Sn},\text{Zr})_2\text{O}_7$ pyrochlore, *Phys. Rev. B* **70**, 054110 (2004).
- [18] V. P. Zhukov and V. M. Za, First-principles calculations of the electronic structure of fluorite-type crystals and transport properties, *Phys. Solid State* **40**, 1827 (1998).
- [19] W. Mackrodt, Defect Calculations for Ionic Materials, in *Computer Simulation of Solids* (Springer-Verlag, Berlin, 1982) Chap. 12, p. 175.
- [20] G. A. Samara, Pressure and temperature dependences of the ionic conductivities of cubic and orthorhombic lead fluoride (PbF_2), *J. Phys. Chem. Solids* **40**, 509 (1979).
- [21] Data for this study are available from doi:10.5286/ISIS.E.RB1920547.
- [22] There were some additional sites for $\alpha\text{-PbF}_2$ and YF_3 which had energy only a few meV above these, but the muon polarization due to these sites are not realized in the data. See Supplemental Information for details.